Microstructure, strength and environmental degradation of proppants

E. BREVAL, J. S. JENNINGS, S. KOMARNENI*, N. H. MACMILLAN
Materials Research Laboratory, The Pennsylvania State University, University Park, Pennsylvania 16802, USA

E. P. LUNGHOFER
General Abrasive, Division of Dresser Industries, Inc., 2000 College Avenue, Niagara Falls, New York 14305, USA

The microstructures of four manufactured proppants are described. As-received, all are stronger in diametral compression than quartz sand; and exposure to 3 N NaCl or $MgCl_2$ brines at 423 K and 69 MPa for up to 336 h does not change this. Exposure to 12 wt% HCl + 3 wt% HF at the same temperature and pressure reduces the strengths of the manufactured proppants faster than that of sand. The rate of loss of strength depends on the ratio of proppant to acid present during hydrothermal treatment. After a few hours, however, only the strongest and most acid-resistant manufactured proppants retain any significant strength advantage over sand.

1. Introduction

Proppants are millimetre-size ceramic particles used to "prop open" hydrofractured oil wells. To be effective they should be strong and should break into few fragments. They also should be accurately spherical and uniform in size to ensure that they flow readily. In addition, they need to be able to resist at elevated temperatures and pressures both the ground waters (brines) found in deep wells and the HF–HCl mixtures sometimes pumped into such wells to clear blockages. Finally, they should be cheap. For this last reason, grains of (α-) quartz sand are widely used as proppants. Recently, however, the search for superior properties has led to the development of a variety of manufactured proppants. This paper describes the microstructures of four such proppants and compares their mechanical properties with those of quartz sand grains both before and after hydrothermal treatment in 3 N NaCl and $MgCl_2$ brines and in a 12 wt% HCl + 3 wt% HF solution.

2. Experimental materials

2.1. Methods of characterization

Figs 1a to d show the four manufactured proppants, hereinafter designated I, II, III, and IV, respectively; and Fig. 1e shows the quartz sand. The surface textures of all five proppants were investigated by optical and scanning electron microscopy (SEM) both as-received and (when possible) after various hydrothermal treatments. Additional characterization studies carried out on the as-received proppants included: (i) wet chemical analyses; (ii) SEM investigations of pore structures as seen in polished cross-sections; (iii) mercury porosimetry measurements of pore volumes and pore size distributions; (iv) X-ray powder diffraction (XRD) investigations of phase compositions; (v) transmission electron microscopic (TEM) examinations and energy-dispersive X-ray spectroscopic (EDS) analyses of ion-beam thinned foils; and (vi) measurements of density by pycnometry. Finally, size and shape factors Δ_1 and Δ_2, respectively, were calculated for each proppant in the as-received condition from measurements of the largest (d_{max}) and the smallest (d_{min}) diameters of a number (n = 15 to 20) of particles. Δ_1, which is an indicator of size variation, is defined as

$$\Delta_1 = \frac{1}{n}\sum_{i=1}^{n}\left|\frac{d^i_{max} + d^i_{min}}{\bar{D}} - 1\right|$$

where

$$\bar{D} = \frac{1}{n}\sum_{i=1}^{n}(d^i_{max} + d^i_{min})$$

and Δ_2, which is an indicator of shape variation, is defined as

$$\Delta_2 = \frac{2}{n\bar{D}}\sum_{i=1}^{n}(d^i_{max} - d^i_{min})$$

If all the particles are perfect spheres of exactly the same radius, $\Delta_1 = \Delta_2 = 0$. If the size varies but the shape does not, Δ_2 remains zero but Δ_1 increases as the size distribution broadens. Conversely, if the mean diameter (size) remains constant (i.e. $d^i_{max} + d^i_{min} = \bar{D}$ for all i) but the shape varies, Δ_1 remains zero but Δ_2 increases as d_{max} and d_{min} diverge.

2.2. Macrostructure

Figs 1a to e and the values of Δ_1 and Δ_2 listed in Table I reveal that Proppants III and IV are both the most uniform in size and the most nearly spherical.

*Also associated with the Department of Agronomy.

0022–2461/87 $03.00 + .12

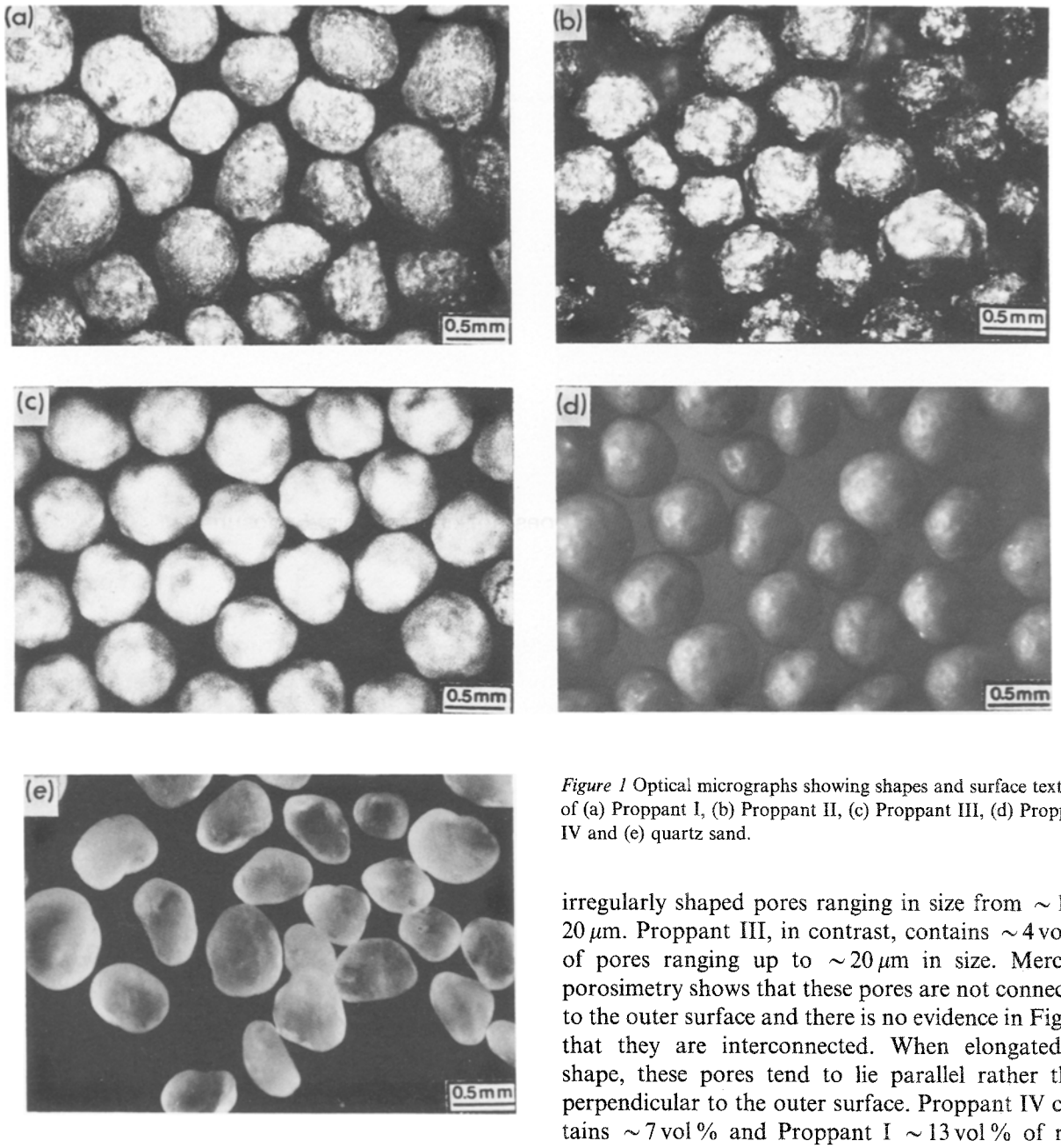

Figure 1 Optical micrographs showing shapes and surface textures of (a) Proppant I, (b) Proppant II, (c) Proppant III, (d) Proppant IV and (e) quartz sand.

For the remaining proppants, regularity of shape decreases in the sequence Proppant II, Proppant I, sand; but there is no concomitant variation in uniformity of size.

Lineal analyses of the polished cross-sections shown in Figs 2a to e and the mercury porosimetry measurements reveal that all five proppants contain rather different distributions of pores. The quartz sand grains contain less than 1 vol % of apparently isolated, irregularly shaped pores ranging in size from ~ 1 to $20\,\mu m$. Proppant III, in contrast, contains ~ 4 vol % of pores ranging up to $\sim 20\,\mu m$ in size. Mercury porosimetry shows that these pores are not connected to the outer surface and there is no evidence in Fig. 2c that they are interconnected. When elongated in shape, these pores tend to lie parallel rather than perpendicular to the outer surface. Proppant IV contains ~ 7 vol % and Proppant I ~ 13 vol % of randomly distributed pores which range widely in size. The longest dimension of the largest pores approaches $100\,\mu m$ in Proppant I and $20\,\mu m$ in Proppant IV. Both Fig. 2a and the mercury porosimetry data suggest that these pores are closed and isolated. In the case of Proppant II the porosity is ~ 17 vol %. The pores range in size from ~ 5 to $40\,\mu m$ and are more regularly distributed than the pores in Proppant I. Again there is no evidence that the pores are connected either to the outer surface or to one another (Fig. 2b). The

TABLE I Characteristics of proppants

Proppant	Density (10^3 kg m^{-3})	Porosity (vol %)	Chemical composition (wt%) (major constituents only)			Phase composition (major constituents only)	Size factor, Δ_1	Shape factor, Δ_2
			SiO_2	Al_2O_3	Fe_2O_3			
I	3.19	12.8	14.2	75	5.8	Corundum + mullite + SiO_2 glass	0.10	0.26
II	3.24	16.7	13.5	75	5.5	Corundum + mullite + SiO_2 glass	0.10	0.16
III	2.72	4.3	44	51	1.5	~ 71 wt % mullite + cristobalite + SiO_2 glass*	0.03	0.07
IV	2.90	6.9	35	58.8	3.3	~ 82 wt% mullite + SiO_2 glass*	0.05	0.06
Sand	2.67	< 1	Not determined			$\sim 100\%$ α-quartz	0.09	0.34

*Assuming all Al_2O_3 present in mullite.

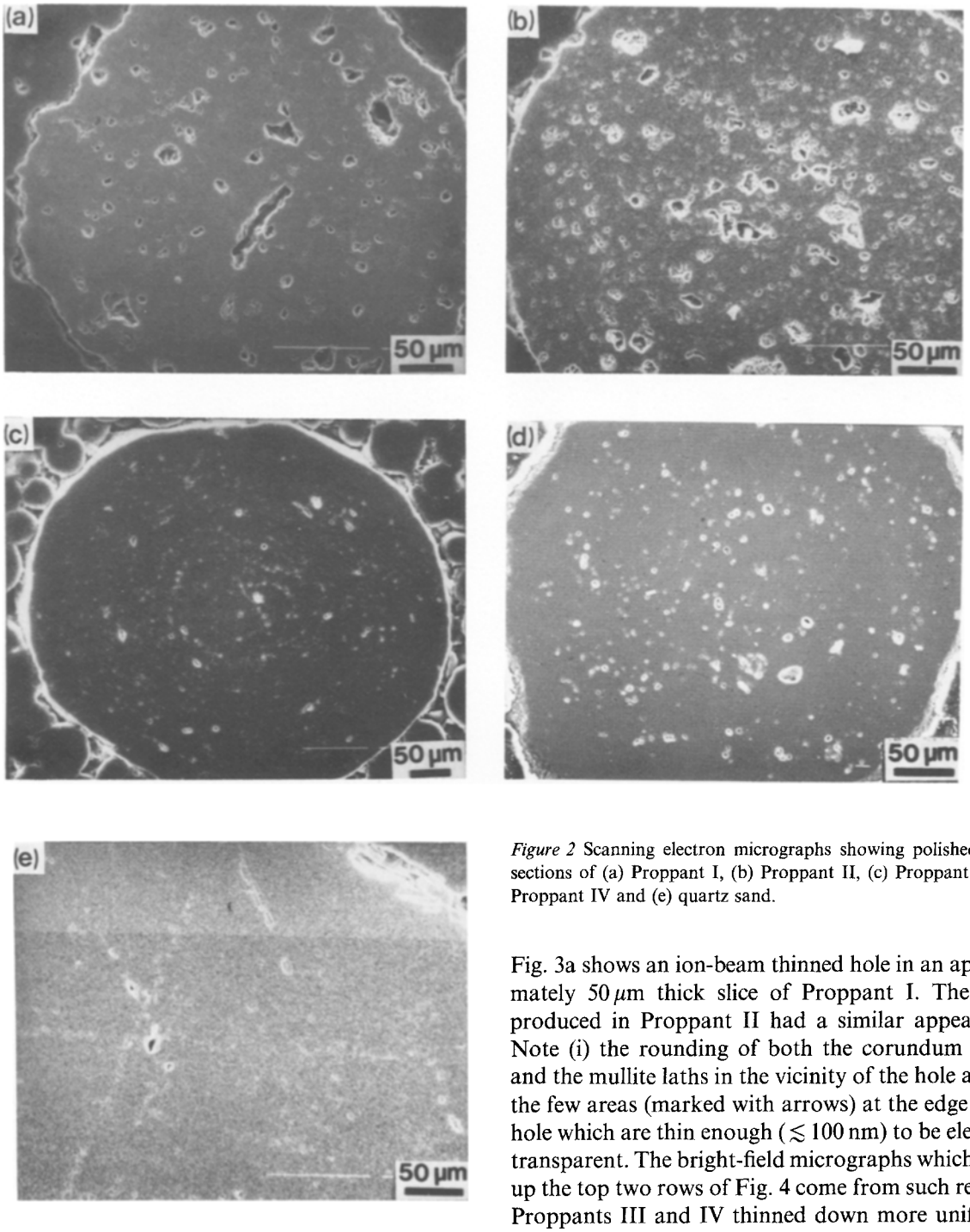

Figure 2 Scanning electron micrographs showing polished cross-sections of (a) Proppant I, (b) Proppant II, (c) Proppant III, (d) Proppant IV and (e) quartz sand.

measured porosities are listed in Table I, together with the results of the density measurements. Also listed in Table I are the results of wet chemical analyses for the major elements (aluminium, silicon and iron) and of X-ray diffraction studies of phase composition. These last studies reveal that Proppants I and II both contain mullite ($3Al_2O_3 \cdot 2SiO_2$) and corundum. However, Proppant II contains more mullite than Proppant I. Proppant III contains mullite and α- and β-cristobalite; Proppant IV contains mullite exclusively; and the sand is α-quartz.

2.3. Microstructure

Detailed TEM investigations were undertaken to determine the microstructures of all five proppants. Such a study is not trivial to perform because neither chemical dissolution nor ion-beam thinning removes all microstructural constituents at the same rate. Fig. 3a shows an ion-beam thinned hole in an approximately 50 μm thick slice of Proppant I. The holes produced in Proppant II had a similar appearance. Note (i) the rounding of both the corundum grains and the mullite laths in the vicinity of the hole and (ii) the few areas (marked with arrows) at the edge of the hole which are thin enough ($\lesssim$ 100 nm) to be electron-transparent. The bright-field micrographs which make up the top two rows of Fig. 4 come from such regions. Proppants III and IV thinned down more uniformly by virtue of their finer grain sizes. Fig. 3b shows along its left margin the edge of an ion-beam thinned hole in a thin slice of Proppant III. Despite the poor contrast and low magnification, the uniform distribution of the sub-micrometre grains can be seen. Some enlargement of the pores by the ion-beam thinning process is also evident. The middle row of micrographs in Fig. 4 comes from the edge of the large hole on the left in Fig. 3b, and the fourth row comes from the edge of a similar hole in a thin slice of Proppant IV. By virtue of their single-crystal nature, the sand grains could be ion-beam thinned without difficulty; micrographs from electron-transparent regions form the bottom row of Fig. 4.

Fig. 4 shows that the coarse (2 to 10 μm) corundum and mullite grains in Proppant I (Fig. 3a) are bound together by a glassy phase containing fine (200 to 1000 nm) angular grains of corundum and a large volume fraction of finer (10 to 50 nm) mullite grains of

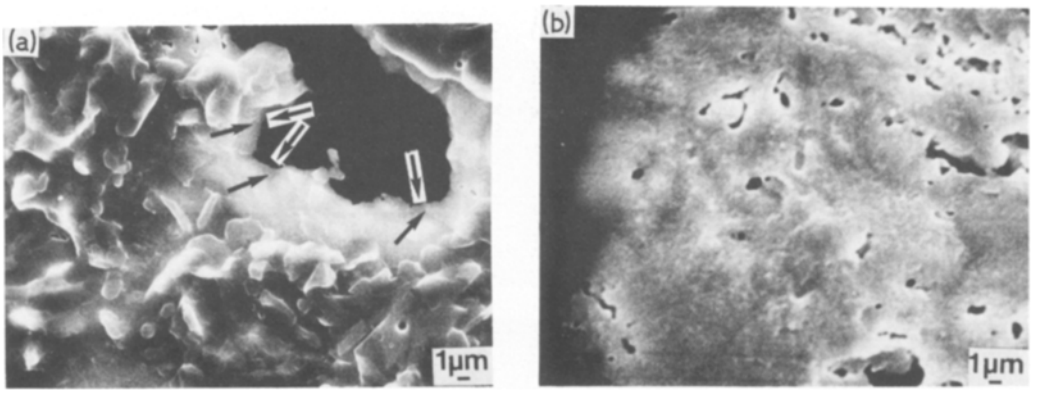

Figure 3 Ion-beam thinned holes in proppants. Proppants I and II form rough surfaces as shown in (a), from Proppant I. Proppants III and IV form smooth surfaces as shown in (b), from Proppant III.

rounder morphology. This glassy phase consists mostly of SiO_2, though it contains aluminium in some regions. It also exhibits evidence of crystallinity in some places. The glassy phase binding together the coarse corundum and mullite grains in Proppant II also contains fine grains of corundum and mullite. The former range in size from 200 to 2000 nm and are more rounded than their analogues in Proppant I; and the latter exhibit a similar morphology and range in size from 200 to 500 nm. Some areas of this glassy binder phase also contain tiny (2 to 20 nm) crystals of β-cristobalite. The primary constituent of Proppants III and IV is 200 to 1000 nm angular grains of mullite. These are bonded together by an SiO_2-rich glass which in the case of Proppant III contains heavily twinned 10 to 50 nm crystals of α-cristobalite and a small and unevenly distributed amount of β-cristobalite (none visible in Fig. 4). In Proppant IV the glassy binder phase appears to be everywhere amorphous and free of cristobalite, even in the dark regions. The sand grains are composed of subgrains ranging in size from a few to a few hundred micrometres and separated by low-angle grain boundaries (arrowed). Consequently they exhibit undulating extinction when rotated between crossed polars in a polarized light microscope. Also arrowed in Fig. 4 are a few isolated dislocations within individual subgrains.

3. Experimental methods

3.1. Hydrothermal treatment

All hydrothermal treatments were carried out in sealed gold capsules at 423 K and 69 MPa, using cold-seal pressure vessels. The solutions were all aqueous – either 3 N NaCl, 3N $MgCl_2$ or a mixture of 12 wt % HCl + 3 wt % HF. Treatment times were 336 h in the first two of these environments and ranged from 15 min to 48 h in the third.

Because it is metastable, the glassy binder phase present in the manufactured proppants is the microstructural constituent most likely to corrode under hydrothermal conditions. The majority of the hydrothermal treatments were therefore carried out at a proppant to solution ratio of 200 mg ml^{-1}. Assuming complete ionization, 3 N NaCl, 3N $MgCl_2$ and 12 wt % HCl + 3 wt % HF solutions contain 106.5 mg ml^{-1} Cl^-, 106.5 mg ml^{-1} Cl^-, and 117 mg ml^{-1} Cl^- + 29 mg ml^{-1} F^- respectively. Thus, if one Al^{3+} ion needs to react with three halide ions and one Si^{4+} ion needs to react with four halide ions to get into solution, these solutions have the potential to dissolve either 21, 21 and 34 mg ml^{-1} Si or 27, 27 and 43 mg ml^{-1} Al, respectively, always assuming, of course, that the proposed reaction is thermodynamically possible*. Now, from Table I, the glass content of Proppant I or II cannot exceed ~ 14 wt %; the actual glass content is probably significantly less than this because mullite is present in sufficient quantity to be clearly visible in the X-ray diffraction pattern. In the case of Proppants III and IV, all of the Al_2O_3 is present as mullite. Hence 20 wt % of the 44 wt % SiO_2 present in Proppant III is bound up in mullite, leaving no more than 24 wt.% as glass. Even this latter figure is an overestimate because crystalline cristobalite is also present. For Proppant IV, 23 wt % SiO_2 is bound up in mullite, leaving 12 wt % as glass. Thus, 200 mg of Proppant I or II contain ~ 13 mg Si; and a similar quantity of Proppant III or IV contains $\lesssim$ 21 mg Si or ~ 11 mg Si, respectively. Hence, 1 ml of any of the test solutions is theoretically sufficient to consume all of the glassy binder when reaction is thermodynamically possible; but in no case is this quantity of solution able – even in theory – to consume the whole proppant.

To see what happens when the ratio of proppant to solution is decreased to a value such that the solution theoretically can consume the entire mass of proppant, a parallel series of experiments was performed in the acid environment at the same temperature and pressure using a proppant to solution ratio of 10 mg ml^{-1}.

3.2. Mechanical testing

The strengths of all five proppants were determined both before and after hydrothermal treatment by diametrally compressing spheres one at a time between WC–Co anvils on an Instron universal testing machine [1–3]. Eight to twelve spheres of each type were tested in each condition at a crosshead speed of 5×10^{-3} cm min^{-1}. In each case the fracture surface and the shapes of the fragments were examined by SEM.

*Reactions such as $Si^{4+} + 6X^- \rightarrow SiX_6^{2-}$ are ignored as they consume less silicon per unit volume of solution.

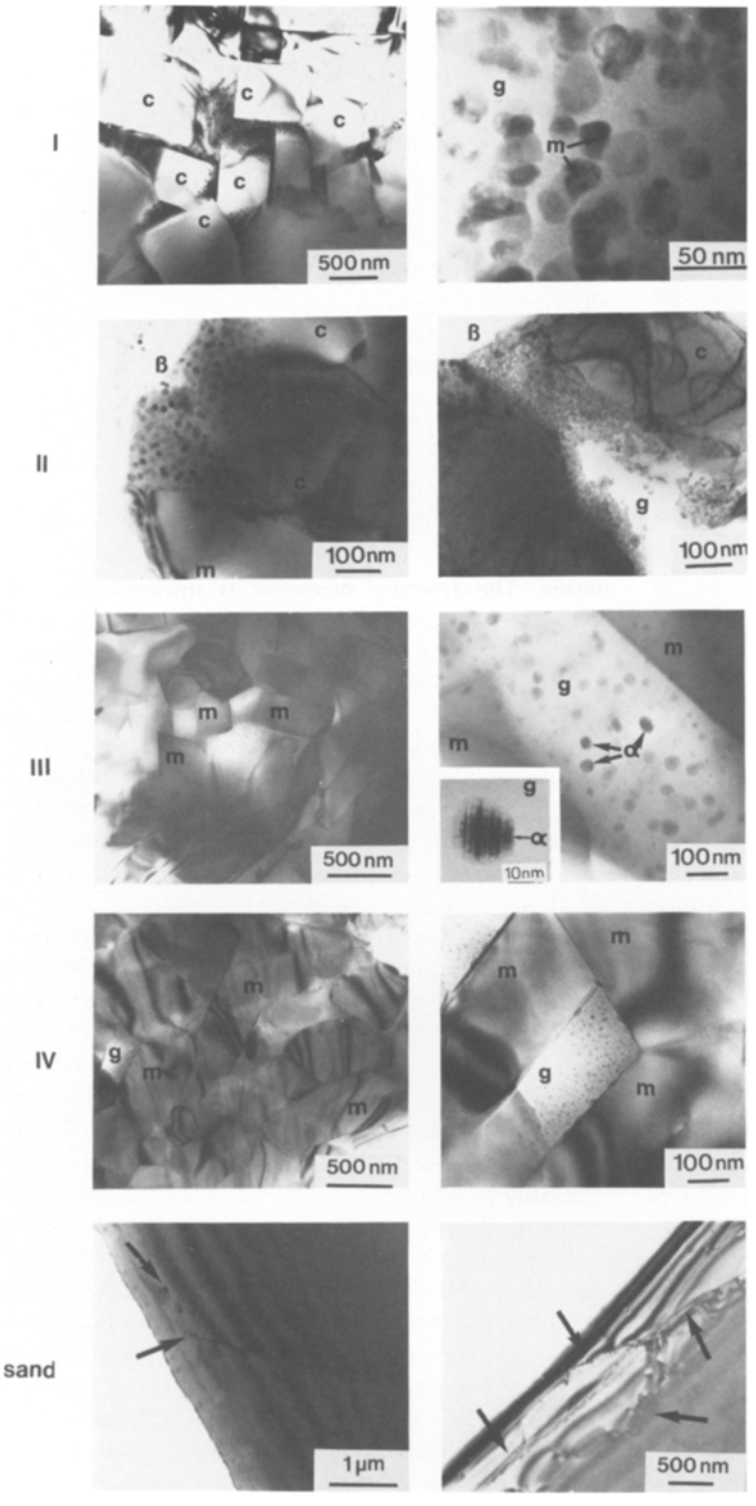

Figure 4 Transmission electron micrographs of ion-beam thinned sections of Proppants I, II, III, and IV and of quartz sand: c = corundum, m = mullite, g = glassy matrix, α = α-cristobalite, β = β-cristobalite. The low-angle grain boundaries and isolated dislocations in quartz sand are marked with arrows.

Figs 5a and b show the geometry of the diametral compression test and the load (P) against displacement (Z) curve typically obtained from such a test. P_1 and Z_1 are the load and displacement at fracture, and R is an average radius obtained by measuring 3 to 6 randomly selected diameters of about 40 randomly selected spheres of each kind with a micrometer. It has been shown [1–3] that the highest tensile stresses σ_x and σ_y occur at the centre in the case of a sphere made of a homogeneous isotropic linear elastic material. These stresses act radially in the plane perpendicular to the axis of compression (z) and are given by

$$\sigma_x = \sigma_y = \frac{P}{\pi R^2}\left(\frac{21}{28 + 20\nu}\right) \quad (1)$$

where ν is Poisson's ratio. If the origin of the Cartesian coordinates x, y, z is placed at the centre of the sphere, σ_x and σ_y are found to vary very little with position along the z axis in the interval $-0.5R < z < 0.5R$ [3]. The compressive stress σ_z at the centre is given by

$$\sigma_z = -\frac{P}{\pi R^2}\left(\frac{42 + 15\nu}{14 + 10\nu}\right) \quad (2)$$

This is the smallest value of σ_z at any point along the load axis [3]. For present purposes ν can be taken as 0.25, which value is typical for a ceramic material. The error arising from this assumption should not be large because σ_x ($= \sigma_y$) and σ_z are only slowly varying functions of ν.

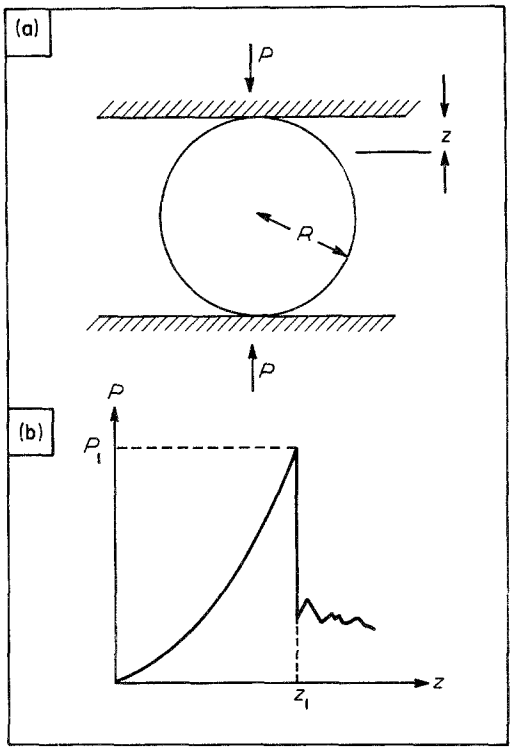

Figure 5 (a) Diametral compression test geometry and (b) typical load–displacement curve.

4. Results

Table II summarizes the results of the diametral compression tests. All four manufactured proppants have higher load-carrying capacities P_1 in the as-received condition than does the quartz sand; and the load-carrying capacities of Proppants I to III and sand remain unaffected after 336 h exposure to 3 N NaCl or 3 N $MgCl_2$ solutions at 423 K and 69 MPa. There is no reason to believe that Proppant IV would behave any differently. In contrast, at both ratios of proppant to solution, exposure to 12 wt % HCl + 3 wt % HF at the same temperature and pressure reduces the load-carrying capacities of all four manufactured proppants more rapidly than that of sand. When the proppant to solution ratio is such that only the glassy binder phase can be consumed, Proppants I and II lose virtually all of their load-carrying capacity within 6 h. In contrast, Proppants III and IV still retain about one-third of their load-carrying capacities after 48 h exposure; and sand retains about one-half of its load-carrying capacity after similar exposure. At the lower proppant to solution ratio, Proppants I and II are reduced to loose debris within 1 h, while Proppants III and IV and sand all retain about one-half of their original load-carrying capacities after 1 h exposure.

Figs 6a to e show that in the as-received condition all five kinds of sphere fractured across one or two vertical diametral planes into two or three large fragments. In addition, local crushing at the points of contact with the anvils produced a very small amount of micrometre-size or finer debris. Figs 7a to e are higher-magnification micrographs of the same fracture surfaces. In the case of Proppant I fracture is partly intergranular and partly intragranular, whereas in Proppant II it appears to be largely intragranular. In both cases the maximum grain size is some micrometres. The fracture probably is intragranular in Proppant III also, but in this case the sub-micrometre grain size makes it difficult to resolve details of the fracture surface topography. The fracture surface is noticeably smoother than those of the other manufactured proppants. In Proppant IV the fracture appears to be partly intergranular and partly intragranular; and the quartz sand exhibits a typical conchoidal fracture. The mode of fracture and the fracture surfaces of spheres treated in the 3 N NaCl or 3 N $MgCl_2$ solutions appear no different.

Fracture surfaces of spheres broken following hydrothermal treatment in 12 wt % HCl + 3 wt % HF for 24 h at a proppant to solution ratio of 200 mg ml^{-1} are shown in Figs 8a to e. In the case of quartz sand, fracture occurred across one or two vertical diametral planes and the fracture surface shows that the acid penetrated only to a depth of a few tens of micrometres. Proppants I, II and III also fractured on vertical diametral planes. In each case the fracture surface is rougher than that of the corresponding proppant tested as-received or after exposure to 3 N NaCl or 3 N $MgCl_2$. As in these latter environments, however, Proppant III still exhibits a smoother fracture surface than do Proppants I and II. Because the microtopographies of the fracture surfaces of acid-treated Proppants I, II, and III appear the same at all points, it is

TABLE II Load-carrying capacities of proppants

Proppant Diameter (mm)	I 0.65 ± 0.08	II 0.68 ± 0.09	III 0.78 ± 0.06	IV 0.74 ± 0.08	Sand 0.67 ± 0.09
Treatment	Load at fracture (N)				
As-received	73 ± 30	61 ± 12	95 ± 24	115 ± 22	41 ± 11
After 336 h in 3 N NaCl	71 ± 23	73 ± 20	98 ± 24	–	42 ± 14
After 336 h in 3 N $MgCl_2$	70 ± 12	76 ± 18	91 ± 18	–	47 ± 17
In 12 wt % HCl + 3 wt % HF, 200 mg ml^{-1} proppant					
after 6 h	4 ± 3	4 ± 2	76 ± 17	97 ± 20	25 ± 10
after 12 h	2 ± 1	1 ± 1	70 ± 11	95 ± 14	21 ± 8
after 24 h	2 ± 1	14 ± 18	57 ± 21	55 ± 25	36 ± 19
after 48 h	1 ± 1	2 ± 1	39 ± 22	32 ± 40	23 ± 18
In 12 wt % HCl + 3 wt % HF, 10 mg ml^{-1} proppant					
after 0.25 h	10 ± 4	11 ± 4	90 ± 8	93 ± 9	35 ± 9
after 1 h	0*	1 ± 1	40 ± 21	67 ± 35	26 ± 11

*Load at fracture too small to measure.

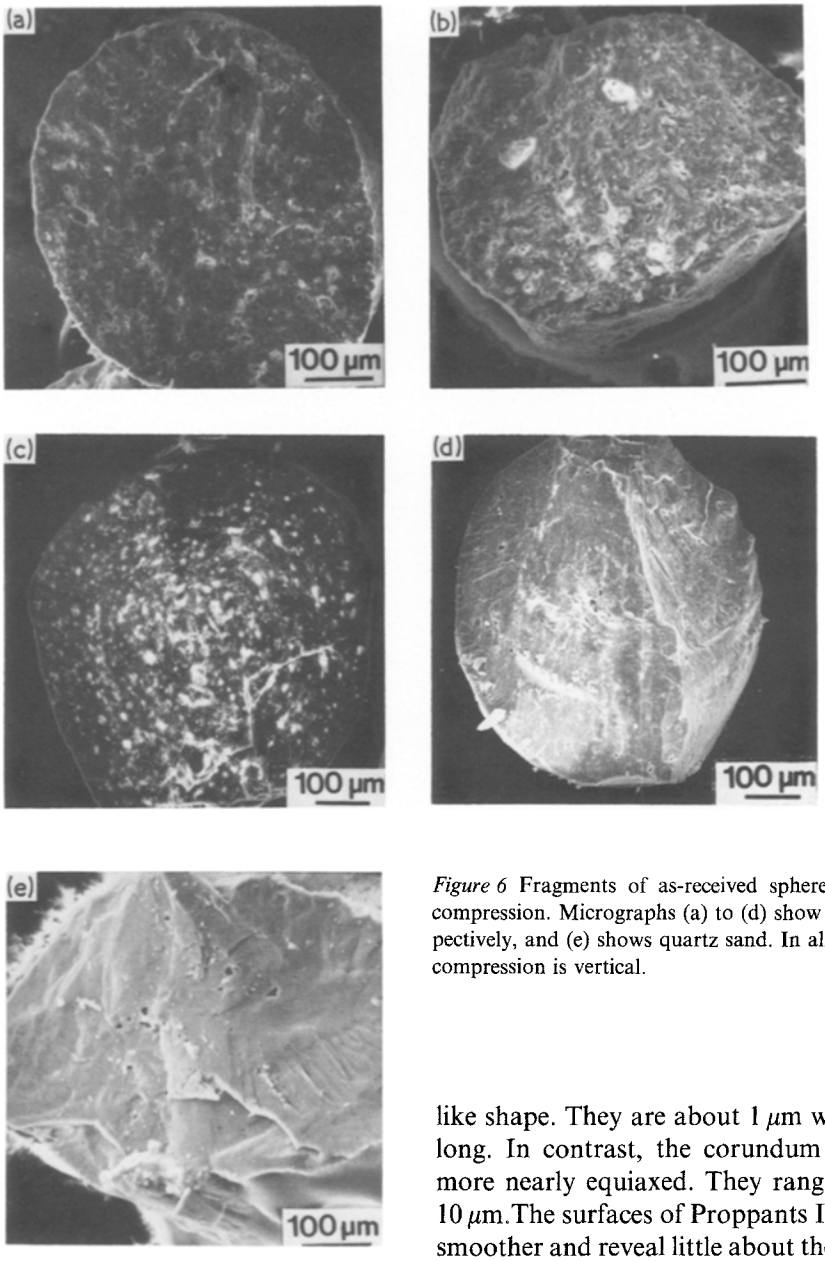

Figure 6 Fragments of as-received spheres broken in diametral compression. Micrographs (a) to (d) show proppants I to IV, respectively, and (e) shows quartz sand. In all five figures the axis of compression is vertical.

concluded that the acid penetrated the entire volume of the spheres during the hydrothermal treatment. Proppant IV exhibited a more complex failure. First, an outer layer spalled away to leave an inner core. This core subsequently fractured on one or more vertical diametral planes, producing a rough fracture surface. Fig. 8d shows a core exhibiting two near-diametral fractures and having what may be a small piece of the outer shell still attached (at the top of the figure). Fig. 9 contrasts the failure mode of Proppant IV with that of Proppants I, II and III. The core seen in Fig. 9b is the same one as shown in Fig. 8d. The implication of this fracture behaviour is that the acid did not penetrate uniformly throughout Proppant IV in 24 h at a proppant to solution ratio of 200 mg ml^{-1}.

Fig. 10 shows the outer surfaces of spheres in the as-received condition and after hydrothermal treatment in 3 N $MgCl_2$ for 336 h or in 12 wt % HCl + 3 wt % HF for 24 h. In the as-received condition, the outer surfaces of Proppants I and II reveal the different morphologies of their two primary constituents. The mullite crystals exhibit their characteristic lath-like shape. They are about 1 μm wide and 5 to 10 μm long. In contrast, the corundum crystals are much more nearly equiaxed. They range in size from 1 to 10 μm. The surfaces of Proppants III and IV are much smoother and reveal little about the underlying microstructure; and over most of their surfaces the quartz sand grains show evidence of extensive microchipping, which presumably results from particle–particle contact.

Treatment in 3 N $MgCl_2$ followed by cooling and depressurization only changes these surface morphologies slightly. There is evidence in higher-magnification micrographs of the formation of a very fine precipitate on the surfaces of all the manufactured proppants. This precipitate is thought to be $Mg(OH)_2$ formed by hydrolysis of the $MgCl_2$ [4]. There is no evidence of such precipitation on the surfaces of the quartz grains. Treatment in 12 wt % HCl + 3 wt % HF at a proppant to solution ratio of 200 mg ml^{-1} followed by cooling and depressurization has a far greater effect on surface morphology. The surface of Proppant I exhibits recesses formed by the removal of laths of mullite and evidence of the formation of a precipitate on the protruding grains of corundum. This precipitation is more strongly evident on the surface of Proppant II. The surfaces of Proppants III and IV are covered by micrometre-size spheres and the surface of the quartz sand exhibits extensive etching, pitting and microfissuring.

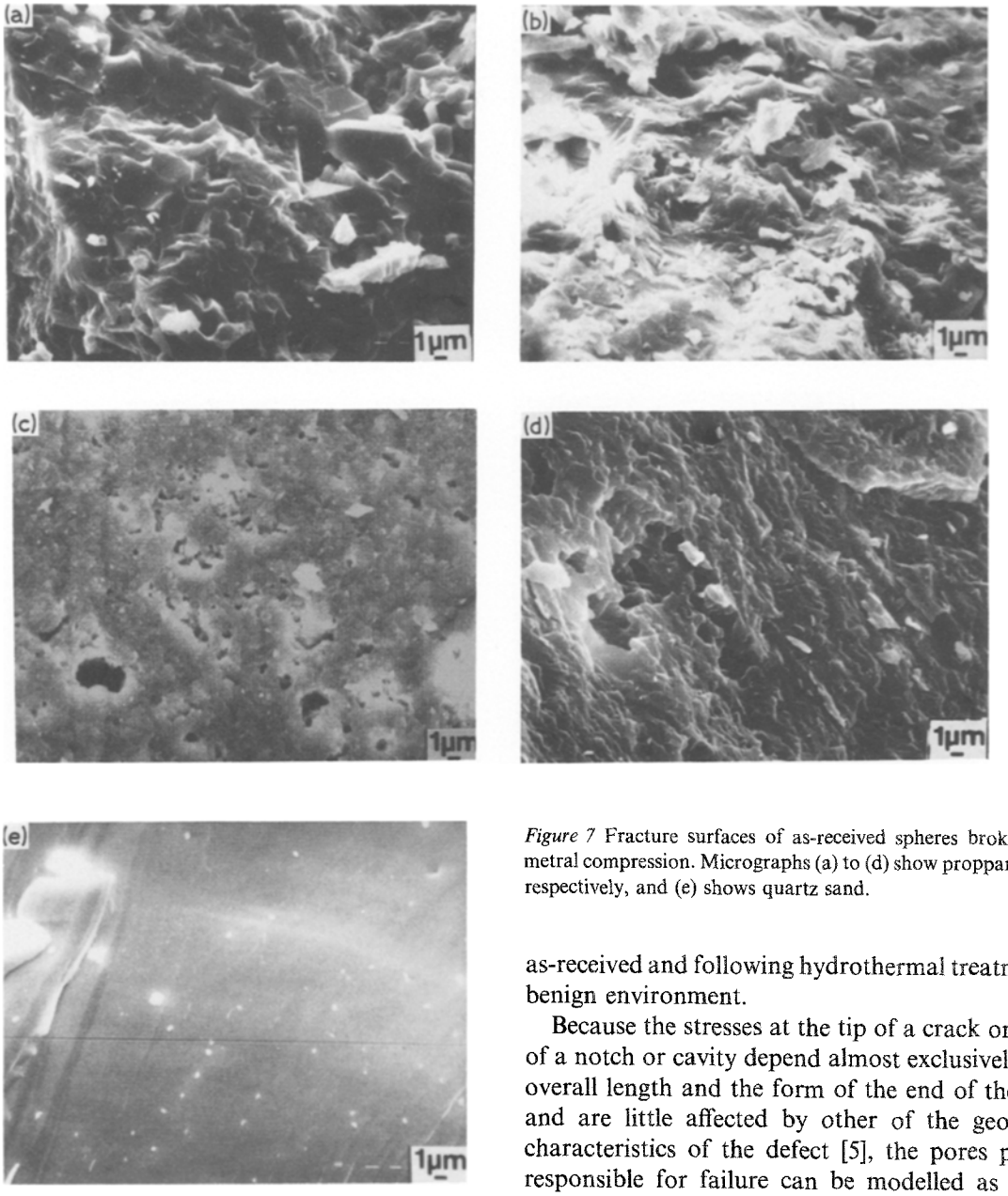

Figure 7 Fracture surfaces of as-received spheres broken in diametral compression. Micrographs (a) to (d) show proppants I to IV, respectively, and (e) shows quartz sand.

5. Discussion

In the as-received condition, all four manufactured proppants have a greater load-carrying capacity than natural, rounded quartz sand grains. This situation is not changed by exposure to 3 N NaCl or 3 N $MgCl_2$ brine at 423 K and 69 MPa for periods up to 336 h. In the same three environmental conditions, all five kinds of sphere fail by brittle fracture on one or two vertical diametral planes. This mode of failure suggests strongly that fracture begins from an internal defect – probably a pore – located somewhere near the centre of the proppant where the tensile stresses are largest. A rough estimate of the tensile stress acting at the centre of each kind of proppant at failure can be obtained by inserting its average radius and the average value of the load it supported immediately prior to failure in each of the three environments (Table II) into Equation 1 with $\nu = 0.25$. The results are summarized in Table III and make the point that Proppant IV is significantly stronger and sand significantly weaker in tension than Proppants I, II, and III, both as-received and following hydrothermal treatment in a benign environment.

Because the stresses at the tip of a crack or the end of a notch or cavity depend almost exclusively on the overall length and the form of the end of the defect, and are little affected by other of the geometrical characteristics of the defect [5], the pores probably responsible for failure can be modelled as disc- or penny-shaped cracks of radius c. Further, because the tensile stress σ ($=\sigma_x = \sigma_y$) causing fracture acts radially and samples all orientations, it is permissible to assume the crack to be oriented perpendicular to this stress and to propagate in Mode I. In this situation, propagation occurs at a value of σ which does not depend on the magnitudes of any stresses (such as σ_z) acting in the plane of the crack. Hence, because $\sigma_x = \sigma_y$ is very nearly constant along the load (z-) axis for $|z| < 0.5R$ [3], it is also permissible to make the simplifying assumption that fracture initiates in a uniform stress field. The analysis of Sack [6] is then applicable, and failure occurs when

$$\sigma = \left(\frac{\pi E\gamma}{2(1-\nu^2)c}\right)^{1/2} = \frac{\pi^{1/2}K_{Ic}}{2c^{1/2}} \qquad (3)$$

TABLE III Tensile strengths and fracture toughnesses of as-received proppants

Property	Proppant				
	I	II	III	IV	Sand
$\sigma_x = \sigma_y$ (MPa)	137	123	126	171	78
K_{Ic} (MPa m$^{1/2}$)	1.5	0.8	0.6	0.6	0.4 to 1.0

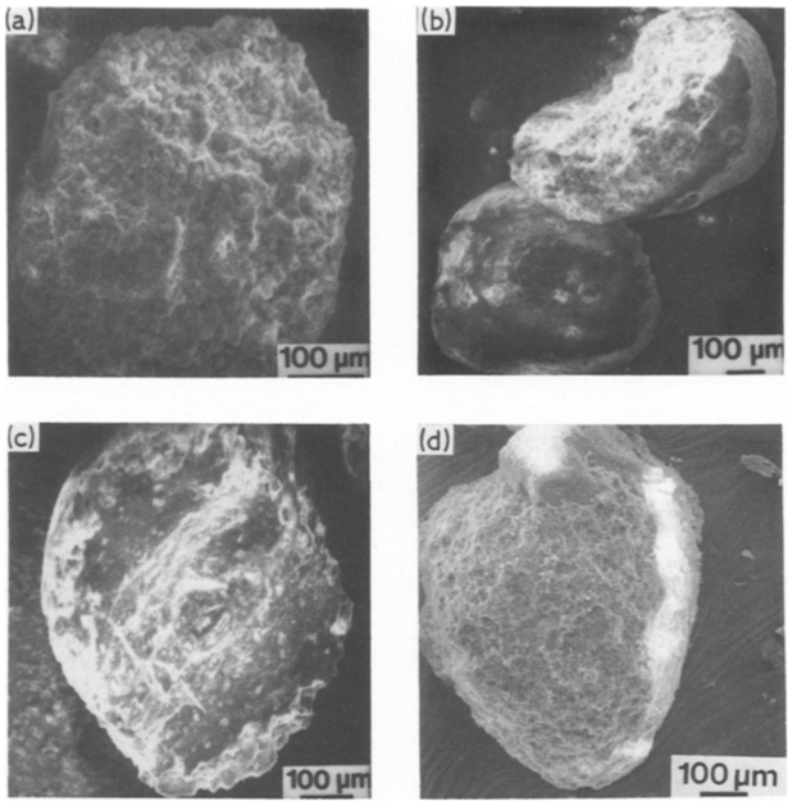

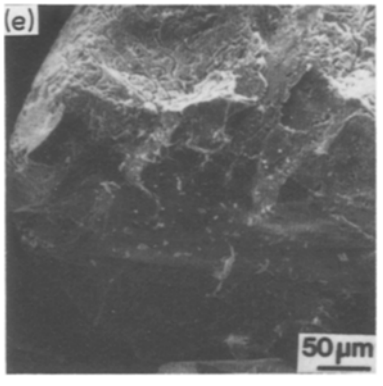

Figure 8 Fragments of spheres broken in diametral compression after hydrothermal treatment in 12 wt % HCl + 3 wt % HF for 24 h at a proppant to solution ratio of 200 mg ml^{-1}. Micrographs (a) to (d) show proppants I to IV, respectively, and (e) shows quartz sand. Proppant IV alone did not show a simple diametral tensile failure. Instead it shed a loose ~20 to 50 μm thick outer layer, exposing a strong inner core. A fragment of this latter is shown in (d). In all five figures the axis of compression is vertical.

where E is Young's modulus, γ is the fracture surface energy and K_{Ic} is the Mode I fracture toughness. Since K_{Ic} for single-crystal quartz has been measured as 0.4 to 1.0 MPa m$^{1/2}$ [7, 8], it follows from Equation 3 that the observed tensile strength of the sand (~ 78 MPa) is controlled by flaws (pores) having a "radius" c of 20 to 140 μm. Pores with dimensions approaching the lower limit of this range are visible in Figs 2e and 6e. Reversing the procedure and inserting values of 100, 40, 20, and 20 μm for c and the strength data from the top row of Table III into Equation 3 yields for Proppants I to IV in the as-received condition the values of K_{Ic} shown in the bottom row of Table III. The values are broadly consistent with the relative roughnesses of the fracture surfaces shown in Figs 7a to d; and they are not unreasonable for SiO_2 glass-bonded materials, since K_{Ic} for different silicate glasses

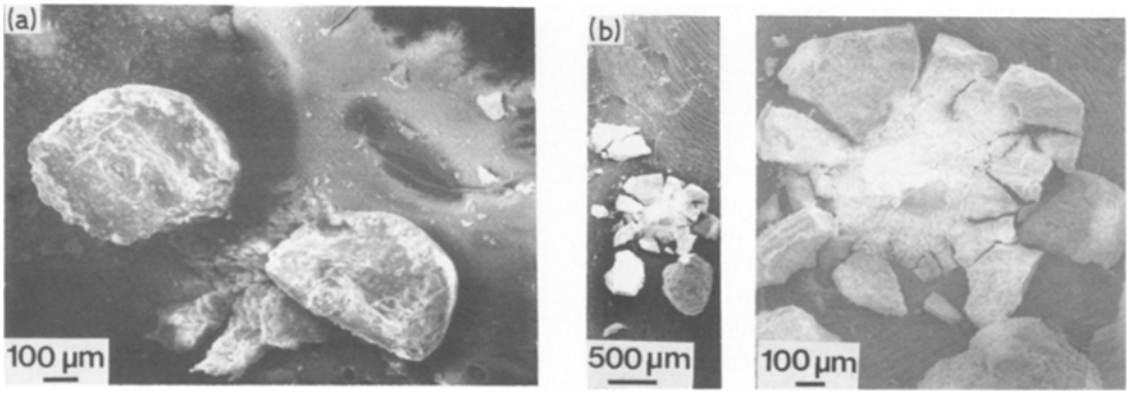

Figure 9 Fracture modes of proppants after hydrothermal treatment in 12 wt % HCl + 3 wt % HF for 24 h at a proppant to solution ratio of 200 mg ml^{-1}. Micrographs (a) shows an example of a diametral fracture, in this case for Proppant III, while (b) shows the more complex fracture mode of Proppant IV, which sheds an outer layer and exposes a strong inner core.

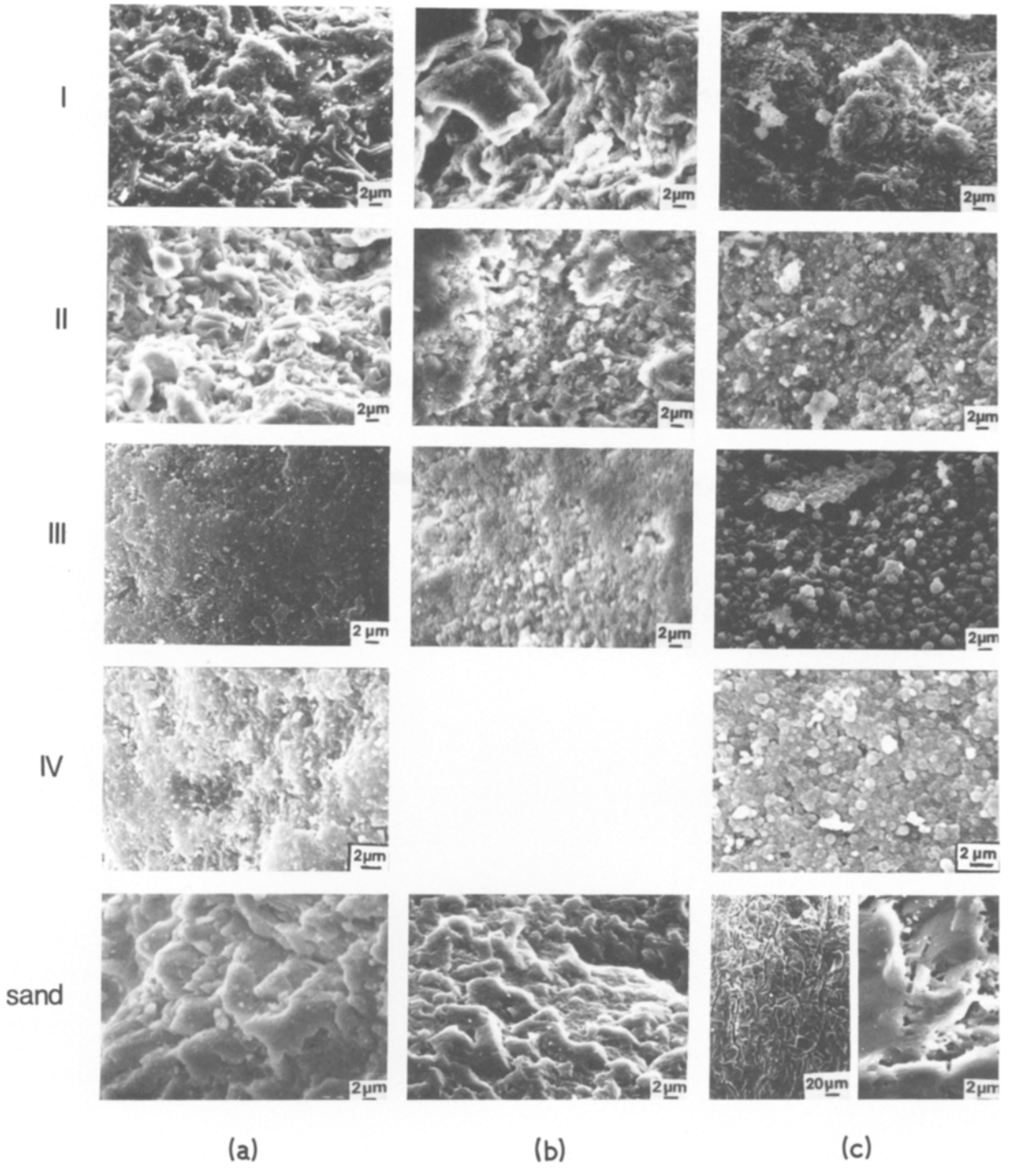

Figure 10 Outer surfaces of spheres (a) as-received and after hydrothermal treatment (b) in 3 N $MgCl_2$ for 336 h and (c) in 12 wt % HCl + 3 wt % HF for 24 h. In both cases the proppant to solution ratio was 200 mg ml^{-1}.

varies between 0.68 and 0.91 MPa $m^{1/2}$ [9]. Kirk and Laird [10] obtained K_{Ic} = 1.8 MPa $m^{1/2}$ for Proppant II by the indentation fracture technique.

Where the strengths of the five proppants studied differ most obviously from one another is in their rates of decrease when exposed to the acid test environment. The degradation process proceeds faster when the ratio of proppant to acid is lower, but for both values of this ratio explored in the present work the relative behaviour of the proppants is the same: sand is more acid-resistant than any of the manufactured proppants, and Proppants III and IV retain useful load-carrying capacities far longer than Proppants I and II. The mechanism of this degradation is taken up in another paper [11].

Acknowledgement

This work was supported by General Abrasive, Division of Dresser Industries, Inc.

References

1. J. N. BRECKER, *J. Eng. Ind. (Trans. ASME B)* **96** (1974) 1253.
2. A. I. LUR'E, "Three-Dimensional Problems in the Theory of Elasticity" (Wiley–Interscience, New York, 1964) pp. 361–367.
3. Y. HIRAMATSU and Y. OKA, *Int. J. Rock Mech. Min.*

Sci. **3** (2) (1966) 89.
4. S. KOMARNENI, *J. Inorg. Nucl. Chem.* **43** (1981) 2833.
5. C. E. INGLIS, *Trans. Inst. Naval Architect.* **55** (1913) 219.
6. R. A. SACK, *Proc. Phys. Soc.* **58** (1946) 729.
7. W. F. BRACE and J. B. WALSH, *Amer. Mineral.* **47** (1962) 1111.
8. B. K. ATKINSON, Final Technical Report for FY 1979, US National Earthquake Hazard Reduction Program (Imperial College, London, UK, 1979) (cited in Landolt-Börnstein, Vol. V/1b, "Physical Properties of Rocks", edited by K.-H. Hellwege, (Springer Verlag, Berlin, 1982) p. 193.
9. S. M. WIEDERHORN, *J. Amer. Ceram. Soc.* **52** (1969) 99.
10. R. S. KIRK and J. A. LAIRD, Paper 201-B-84, American Ceramic Society Annual Meeting, Pittsburgh, Pennsylvania, 1984. Abstract in *Bull Amer. Ceram. Soc.* **63** (1984) 462.
11. S. KOMARNENI, E. BREVAL, J. S. JENNINGS, N. H. MACMILLAN and E. P. LUNGHOFER, *J. Mater. Sci. Lett.* in press.

Received 28 July
and accepted 22 September 1986